Inorg. Chem. **2005**, *44*, 5328–5335

Syntheses, Crystal Structures, and Properties of Six New Lanthanide(III) Transition Metal Tellurium(IV) Oxyhalides with Three Types of Structures

Yue-Ling Shen and Jiang-Gao Mao*

State Key Laboratory of Structure Chemistry, Fujian Institute of Research on the Structure of Matter, The Chinese Academy of Sciences, and the Graduate School of Chinese Academy of Sciences, Fuzhou 350002, P. R. China

Received March 21, 2005

Solid-state reactions of lanthanide(III) oxide (and lanthanide(III) oxyhalide), transition metal halide (and transition metal oxide), and TeO_2 at high temperature lead to six new lanthanide transition metal tellurium(IV) oxyhalides with three different types of structures, namely, $DyCuTe_2O_6Cl$, $ErCuTe_2O_6Cl$, $ErCuTe_2O_6Br$, $Sm_2Mn(Te_5O_{13})Cl_2$, $Dy_2Cu(Te_5O_{13})Br_2$, and $Nd_4Cu(TeO_3)_5Cl_3$. Compounds $DyCuTe_2O_6Cl$, $ErCuTe_2O_6Cl$, and $ErCuTe_2O_6Br$ are isostructural. The lanthanide(III) ion is eight-coordinated by eight oxygen atoms, and the copper(II) ion is five-coordinated by four oxygens and a halide anion in a distorted square pyramidal geometry. The interconnection of Ln(III) and Cu(II) ions by bridging tellurite anions results in a three-dimensional (3D) network with tunnels along the *a*-axis; the halide anion and the lone-pair electrons of the tellurium(IV) ions are oriented toward the cavities of the tunnels. Compounds $Sm_2Mn(Te_5O_{13})Cl_2$ and $Dy_2Cu(Te_5O_{13})Br_2$ are isostructural. The lanthanide(III) ions are eight-coordinated by eight oxygens, and the divalent transition metal ion is octahedrally coordinated by six oxygens. Two types of polymeric tellurium(IV) oxide anions are formed: $Te_3O_8^{4-}$ and $Te_4O_{10}^{4-}$. The interconnection of the lanthanide(III) and divalent transition metal ions by the above two types of polymeric tellurium(IV) oxide anions leads to a 3D network with long, narrow-shaped tunnels along the *b*-axis. The halide anions remain isolated and are located at the above tunnels. $Nd_4Cu(TeO_3)_5Cl_3$ features a different structure. All five of the Nd(III) ions are eight-coordinated (NdO_8 for Nd(1), Nd(2), Nd(4), and Nd(5) and NdO_7Cl for Nd(3)), and the copper(I) ion is tetrahedrally coordinated by four chloride anions. The interconnection of Nd(III) ions by bridging tellurite anions resulted in a 3D network with large tunnels along the *b*-axis. The $CuCl_4$ tetrahedra are interconnected into a 1D two-unit repeating (zweier) chain via corner-sharing. These 1D copper(I) chloride chains are inserted into the tunnels of the neodymium(III) tellurite via Nd–Cl–Cu bridges. Luminescent studies show that $ErCuTe_2O_6Cl$ and $Nd_4Cu(TeO_3)_5Cl_3$ exhibit strong luminescence in the near-IR region. Magnetic measurements indicate the antiferromagnetic interactions between magnetic centers in these compounds.

Introduction

Metal selenites and tellurites can form a variety of unusual structures because of the presence of the stereochemically active lone pair.[1] The asymmetric coordination polyhedron adopted by the Se(IV) or Te(IV) atom may also result in noncentrosymmetric structures with consequent interesting physical properties, such as nonlinear optical second harmonic generation (SHG).[2−4] Transition metal ions with d^0 electronic configuration such as Ti^{4+}, Nb^{5+}, W^{6+}, Mo^{6+}, etc., which are susceptible to second-order Jahn−Teller distor-

* To whom correspondence should be addressed. E-mail: mjg@ms.fjirsm.ac.cn.

(1) (a) Wickleder, M. S. *Chem. Rev.* **2002**, *102*, 2011 (and references therein). (b) Verma, V. P. *Thermochim. Acta* **1999**, *327*, 63 (and references therein).

(2) (a) Ra, H.-S.; Ok, K.-M.; Halasyamani, P. S. *J. Am. Chem. Soc.* **2003**, *125*, 7764. (b) Ok, K.-M.; Halasyamani, P. S. *Inorg. Chem.* **2004**, *43*, 4248. (c) Ok, K.-M.; Orzechowski, J.; Halasyamani, P. S. *Inorg. Chem.* **2004**, *43*, 964. (d) Goodey, J.; Ok, K.-M.; Broussard, J.; Hofmann, C.; Escobedo, F. V.; Halasyamani, P. S. *J. Solid State Chem.* **2003**, *175*, 3.

(3) (a) Hart, R. T.; Ok, K.-M.; Halasyamani, P. S.; Zwanziger, J. W. *Appl. Phys. Lett.* **2004**, *85*, 938. (b) Porter, Y.; Halasyamani, P. S. *J. Solid State Chem.* **2003**, *174*, 441. (c) Goodey, J.; Broussard, J.; Halasyamani, P. S. *Chem. Mater.* **2002**, *14*, 3174. (d) Ok, K.-M.; Halasyamani, P. S. *Chem. Mater.* **2001**, *13*, 4278.

10.1021/ic050420v CCC: $30.25
Published on Web 06/29/2005

tions, have been introduced to the metal selenite or tellurite systems to prepare inorganic materials with good SHG properties.[2−4] Most of such research efforts have been focused on alkali and alkaline earth compounds.[2−4] Although a number of lanthanide selenites and tellurium(IV) oxides have been reported,[1,5,6] reports on lanthanide selenites or tellurium(IV) oxides with additional transition metal ions are still rare.[1,7] Lanthanide compounds such as Er(III) and Nd(III) exhibit good luminescent properties in the near-IR region which have important applications such as an optical signal amplifier;[8] results from our group indicate that some lanthanide tellurium(IV) oxides can also display good luminescent properties in the near-IR region.[6d] Furthermore, the inclusion of magnetic transition metal centers such as copper(II) and manganese(II) ions may lead to compounds with interesting magnetic properties because of 3d−4f magnetic exchange interactions. The inclusion of weak ligands such as halide into the above systems may also result in compounds with new structures and excellent anionic ion-exchange properties. So far only four lanthanide transition metal selenite halides, namely, $SmCo(SeO_3)_2Cl$, $GdCu(SeO_3)_2Cl$, $SmMn(SeO_3)_2Cl$, and $Er_3Cu(SeO_3)_2O_2Cl$ have been structurally characterized; it is reported that the coordination geometry around the transition metal ion plays a subtle role on the structure of the compound formed.[7a,c] To the best of our knowledge, no lanthanide transition metal tellurium(IV) oxyhalides have been structurally characterized. Different from selenium(IV), tellurium(IV) can form a variety of polymeric tellurium(IV) oxide anions; hence a lanthanide transition metal tellurium(IV) oxyhalide system may afford compounds with new structural types as well as novel optical and magnetic properties. Our exploration of lanthanide transition metal tellurium(IV) oxyhalides yielded six new lanthanide transition metal tellurium(IV) oxyhalides, namely, $DyCuTe_2O_6Cl$, $ErCuTe_2O_6Cl$, $ErCuTe_2O_6Br$, $Sm_2Mn(Te_5O_{13})Cl_2$, $Dy_2Cu(Te_5O_{13})Br_2$, and $Nd_4Cu(TeO_3)_5Cl_3$. Herein we report their syntheses, crystal structures, luminescence, and magnetic properties.

Experimental Section

Materials and Instrumentation. All of the chemicals except NdOCl were analytically pure from commercial sources and used without further purification. Transition metal or lanthanide oxides and chlorides were purchased from the Shanghai Reagent Factory; TeO_2 (99+%) was bought from ACROS ORGANICS. NdOCl was synthesized by heating $NdCl_3 \cdot nH_2O$ in air at 400 °C for 12 h, and its purity was checked by X-ray powder diffraction (XRD). The XRD pattern measured is in good agreement with the one simulated from the crystal structure of NdOCl.[9] XRD patterns were collected on a XPERT-MPD $\theta-2\theta$ diffractometer. IR spectra were recorded on a Magna 750 FT-IR spectrometer photometer as KBr pellets in the 4000−400 cm^{-1}. Photoluminescence analyses were performed on an Edinburgh FLS920 fluorescence spectrometer with a microsecond flash lamp (μF900, Edinburgh) as the excitation source. Magnetic susceptibility measurements on polycrystalline samples were performed with a PPMS-9T magnetometer at a field of 10 000 Oe in the range of 2−300 K.

Preparation of $DyCuTe_2O_6Cl$. The single crystals of the title compound (prism in shape and blue in color) were initially prepared by the solid-state reaction of a mixture of Dy_2O_3 (0.112 g, 0.3 mmol), CuO (0.024 g, 0.3 mmol), $CuCl_2$ (0.041 g, 0.3 mmol), and TeO_2 (0.240 g, 1.5 mmol). The reaction mixture was thoroughly ground and pressed into a pellet, which was then sealed into an evacuated quartz tube. Then the quartz tube was heated at 750 °C for 6 days and then cooled to 500 °C at 4.17 °C·h^{-1} before switching off the furnace. After the structural analysis, a pure powder sample of $DyCuTe_2O_6Cl$ was obtained quantitatively by the reaction of a mixture of Dy_2O_3/CuO/$CuCl_2$/TeO_2 in a molar ratio of 1:1:1:4 at 720 °C for 6 days. The purity of $DyCuTe_2O_6Cl$ was confirmed by XRD powder diffraction studies. IR data (KBr, cm^{-1}): 778 (w), 727(m), 696 (m), 658 (s), 476 (m), 452 (w), 412 (w).

Preparation of $ErCuTe_2O_6Cl$ and $ErCuTe_2O_6Br$. Single crystals of $ErCuTe_2O_6Cl$ (prism in shape and light blue in color) and $ErCuTe_2O_6Br$ (prism in shape and light blue in color) were prepared by using a similar procedure to that for $DyCuTe_2O_6Cl$. A pure powder sample of $ErCuTe_2O_6Cl$ was synthesized by the solid-state reaction of a mixture of Er_2O_3/CuO/$CuCl_2$/TeO_2 in a molar ratio of 1:1:1:4 at 720 °C for 6 days. Attempts to obtain a monophase of $ErCuTe_2O_6Br$ were unsuccessful; the reaction product contains Br_2 and some unidentified black powder as impurities. IR data (KBr, cm^{-1}) for $ErCuTe_2O_6Cl$: 778 (w), 728(m), 695 (m), 659 (s), 479 (m), 452 (w), 414 (w).

Preparation of $Sm_2MnTe_5O_{13}Cl_2$ and $Dy_2CuTe_5O_{13}Br_2$. Single crystals of $Sm_2MnTe_5O_{13}Cl_2$ (prism in shape and pink in color) and $Dy_2CuTe_5O_{13}Br_2$ (prism in shape and yellow-green in color) were obtained from the solid-state reaction of a mixture containing 0.3 mmol of Sm_2O_3 (0.104 g, or 0.112 g of Dy_2O_3 for $Dy_2CuTe_5O_{13}Br_2$), 0.3 mmol of MnO_2 (0.026 g, or 0.024 g of CuO for $Dy_2CuTe_5O_{13}Br_2$), 0.3 mmol of $MnCl_2$ (0.038 g or 0.068 g of $CuBr_2$ for $Dy_2CuTe_5O_{13}Br_2$), and 1.8 mmol of TeO_2 (0.287 g) at 750 °C for 6 days. A pure powder sample of $Sm_2MnTe_5O_{13}Cl_2$ was prepared quantitatively by reacting a mixture of Sm_2O_3/$MnCl_2$/TeO_2 in a molar ratio of 1:1:5 at 700 °C for 6 days. Attempts to obtain a monophase of $Dy_2CuTe_5O_{13}Br_2$ failed; the reaction product contains Br_2 and another unidentified black powder as impurities. IR data (KBr, cm^{-1}) for $Sm_2MnTe_5O_{13}Cl_2$: 786 (w), 753 (m), 667 (s), 607 (m), 529 (m), 471 (w), 414 (w).

Preparation of $Nd_4CuTe_5O_{15}Cl_3$. Single crystals of $Nd_4CuTe_5O_{15}Cl_3$ (prismatic and purple) were prepared in a method

(4) (a) Harrison, W. T. A.; Dussack, L. L.; Jacobson, A. J. *J. Solid State Chem.* **1996**, *125*, 234. (b) Johnston, M. G.; Harrison, W. T. A. *Inorg. Chem.* **2001**, *40*, 6518. (c) Balraj, V.; Vidyasagar, K. *Inorg. Chem.* **1999**, *38*, 5809. (d) Balraj, V.; Vidyasagar, K. *Inorg. Chem.* **1999**, *38*, 3458.

(5) (a) Wontcheu, J.; Schleid, T. *J. Solid State Chem.* **2003**, *171*, 429. (b) Wontcheu, J.; Schleid, T. *Z. Anorg. Allg. Chem.* **2002**, *628*, 1941. (c) Ruck, M.; Schmidt, P. *Z. Anorg. Allg. Chem.* **2003**, *629*, 2133. (d) Wontcheu, J.; Schleid, T. *Z. Anorg. Allg. Chem.* **2003**, *629*, 1463. (e) Krugermann, I.; Wickleder, M. S. *J. Solid State Chem.* **2002**, *167*, 113. (f) Krugermann, I.; Wickleder, M. S. *Z. Anorg. Allg. Chem.* **2002**, *628*, 147.

(6) (a) Meier, S. F.; Schleid, T. *Z. Anorg. Allg. Chem.* **2002**, *628*, 1941. (b) Ljjaali, I.; Flaschenrien, C.; Ibers, J. A. *J. Alloys Compd.* **2003**, *354*, 115. (c) Weber, F. A.; Meier, S. F.; Schleid, T. *Z. Anorg. Allg. Chem.* **2001**, *627*, 2225. (d) Shen, Y. L.; Mao, J. G. *J. Alloys Compd.* **2004**, *385*, 86.

(7) (a) Wickleder, M. S.; Hamida, M. B. *Z. Anorg. Allg. Chem.* **2003**, *629*, 556. (b) Harrison, W. T. A.; Zhang, Z. H. *J. Solid State Chem.* **1997**, *133*, 572. (c) Berrigan, R.; Gatehouse, B. M. *Acta Crystallogr.* **1996**, *C52*, 496. (d) Ok, K. M.; Zhang, L.; Halasyamani, P. S. *J. Solid State Chem.* **2003**, *175*, 264.

(8) (a) Slooff, L. H.; Polman, A.; Oude Wolbers, M. P.; van Veggel, F. C. J. M.; Reinhoudt, D. N.; Hofstraat, J. W. *J. Appl. Phys.* **1997**, *83*, 497. (b) Slooff, L. H.; Polman, A.; Klink, S. I.; Hebink, G. A.; Grave, L.; van Veggel, F. C. J. M.; Reinhoudt, D. N.; Hofstraat, J. W. *Opt. Mater.* **2000**, *14*, 101.

(9) Meger, G.; Schleid, T. *Z. Anorg. Allg. Chem.* **1986**, *533*, 181.

Table 1. Crystal Data and Structure Refinements for the Six Compounds

formula	$DyCuTe_2O_6Cl$	$ErCuTe_2O_6Cl$	$ErCuTe_2O_6Br$	$Sm_2MnTe_5O_{13}Cl_2$	$Dy_2CuTe_5O_{13}Br_2$	$Nd_4CuTe_5O_{15}Cl_3$
formula weight	612.69	617.45	661.91	1272.54	1394.36	1624.85
crystal system	monoclinic	monoclinic	monoclinic	monoclinic	monoclinic	monoclinic
space group	*P*2(1)/*c*	*P*2(1)/*c*	*P*2(1)/*c*	*P*2(1)/*n*	*P*2(1)/*n*	*I*2
a/Å	5.3918(14)	5.3845(4)	5.392(2)	15.202(4)	15.397(4)	17.719(8)
b/Å	14.932(4)	14.9040(12)	14.918(6)	5.5801(13)	5.4637(13)	5.663(2)
c/Å	9.110(3)	9.1079(5)	9.317(4)	17.982(4)	17.838(5)	19.39(1)
α/deg	90	90	90	90	90	90
β/deg	98.685(2)	98.684(3)	97.670(4)	104.286(3)	104.577(2)	103.575(3)
γ/deg	90	90	90	90	90	90
V/Å^3	725.0(3)	722.54(9)	742.7(5)	1478.2(6)	1452.3(6)	1891.4(13)
Z	4	4	4	4	4	4
D c/g·cm^{-3}	5.613	5.676	5.920	5.718	6.377	5.706
μ (Mo Kα)/mm^{-1}	21.391	22.738	27.142	18.779	27.047	19.943
goodness-of-fit on F^2	1.084	1.132	1.122	1.050	1.100	1.003
R1, wR2 [$I > 2\sigma(I)$][a]	0.0192, 0.0458	0.0637, 0.1271	0.0304, 0.0716	0.0282, 0.0634	0.0317, 0.0761	0.0304, 0.0550
R1, wR2 (all data)	0.0210, 0.0466	0.0863, 0.1395	0.0321, 0.0728	0.0336, 0.0656	0.0378, 0.0795	0.0364, 0.0576

[a] $R1 = \sum||F_o| - |F_c||/\sum|F_o|$, $wR2 = \{\sum w[(F_o)^2 - (F_c)^2]^2/\sum w[(F_o)^2]^2\}^{1/2}$.

similar to that for $ErCuTe_2O_6Cl$ by using Nd_2O_3 (0.115 g, 0.34 mmol), CuO (0.027 g, 0.34 mmol), $CuCl_2$ (0.045 g, 0.34 mmol), and TeO_2 (0.326 g, 2.04 mmol). Structural analysis indicated that Cu(II) had been reduced to Cu(I) by reducing TeO_2 (which is oxidized to Te(VI)). A pure powder sample of $Nd_4CuTe_5O_{15}Cl_3$ was then synthesized quantitatively by the reaction of a mixture of $NdOCl/Nd_2O_3/CuCl/TeO_2$ in a molar ratio of 2:1:1:5 at 650 °C for 6 days. IR data (KBr, cm^{-1}): 762 (w), 719 (m), 650 (s), 449 (w), 410 (w).

Single-Crystal Structure Determination. Data collections for the six compounds were performed on a Rigaku Mercury CCD diffractometer or a Siemens Smart CCD (for $ErCuTe_2O_6Cl$) equipped with a graphite-monochromated Mo Kα radiation (λ = 0.71073 Å) at 293 K. All of the data sets were corrected for Lorentz and polarization factors as well as for absorption by Multi-scan[10a] or the *ψ*-scan method (for $ErCuTe_2O_6Cl$). The structures were solved by the direct methods and refined by full-matrix least-squares fitting on F^2 by SHELX-97.[10b] All of the atoms, except O(1), O(2), O(4), and O(6) atoms in $ErCuTe_2O_6Cl$, O(4), O(7), O(8), and O(11) in $Nd_4CuTe_5O_{15}Cl_3$, were refined with anisotropic parameters. The oxygen atoms refined with isotropic thermal parameters show nonpositive displacement parameters when refined anistropically, which is due to the absorption correction problems. The relatively higher R1, wR2 (0.0637 and 0.1271, respectively, for 1386 observed data), and residual peaks (5.03 e Å^{-3}, 0.70 from Er(1)) for $ErCuTe_2O_6Cl$ are due to its poor crystal quality. However, since it is isostructural with $DyCuTe_2O_6Cl$ and $ErCuTe_2O_6Br$, the current refinements are good enough and no attempts were made to collect a better data set. For $Nd_4CuTe_5O_{15}Cl_3$, the use of the centrosymmetric space group (*I*2/*m*) resulted in the disorder of some tellurite groups. Hence, it was refined in the noncentrosymmetric space group *I*2; the noncensymmetric space group is also hinted by a low mean $|E^2 - 1|$ value of 0.80 instead of 0.97 expected for a centrosymmetric space group. The refined value of the Flack absolute structure is −0.02(2), which indicates the correctness of the absolute structure. Refinements for other compounds are pretty good. Crystallographic data and structural refinements for the six compounds are summarized in Table 1. Important bond distances are listed in Table 2. More details on the crystallographic studies as well as atomic displacement parameters are given as Supporting Information.

(10) (a) *CrystalClear*, version 1.3.5; Rigaku Corp.: Woodlands, TX, 1999. (b) Sheldrick, G. M. *SHELXTL, Crystallographic Software Package*, version 5.1; Bruker-AXS: Madison, WI, 1998.

Results and Discussion

Structural Descriptions for $DyCuTe_2O_6Cl$, $ErCuTe_2O_6Cl$, $ErCuTe_2O_6Br$, $Sm_2Mn(Te_5O_{13})Cl_2$, $Dy_2Cu(Te_5O_{13})Br_2$, and $Nd_4Cu(TeO_3)_5Cl_3$. These six compounds represent the first examples of structurally characterized lanthanide(III) transition metal tellurium(IV) oxyhalides. They form three different structural types. The chloride-containing compounds can be obtained as a monophase, but the bromide-containing ones ($ErCuTe_2O_6Br$ and $Dy_2Cu(Te_5O_{13})Br_2$) are difficult to obtain as a mono phase product, probably because of the partial decomposing of the copper(II) bromide under our reaction temperatures.

$DyCuTe_2O_6Cl$, $ErCuTe_2O_6Cl$, and $ErCuTe_2O_6Br$ are isostructural; hence only the structure of $DyCuTe_2O_6Cl$ will be discussed in detail as a representative. The synthesis of $DyCuTe_2O_6Cl$ can be expressed by the following reaction at 750 °C: $Dy_2O_3 + CuCl_2 + CuO + 4TeO_2 \rightarrow 2DyCuTe_2O_6Cl$. The structure of $DyCuTe_2O_6Cl$ features a three-dimensional (3D) network. The Dy(III) ion is eight-coordinated by eight oxygen atoms from six tellurite anions, as shown in Figure 1. The Dy−O distances are in the range of 2.302(3)−2.551(3) Å. The copper(II) ion is in a distorted square pyramidal coordination environment composed of four oxygens from four tellurite groups and a chloride anion. The four oxygen atoms form a square, and the chloride anion resides on the pyramidal position. The Cu−Cl distance of 2.633(2) Å is significantly longer than those of the Cu−O bonds (ranging from 1.907(3) to 2.003(3) Å) (Table 2); hence the square pyramid is severely distorted. Both Te(1) and Te(2) are in a *ψ*-TeO_3 tetrahedral coordination geometry with the fourth coordination site occupied by the lone-pair electrons. The Te−O distances are in the range of 1.870(3)−1.896(3) Å. Bond valence calculations indicate that the Te atoms are in an oxidation state of +4; the calculated total bond valences for Te(1) and Te(2) are 3.86 and 3.90, respectively.[11]

Both tellurite groups adopt a same coordination mode, each of them chelates with a Dy(III) ion bidentately and also bridges to two Dy(III) and two Cu(II) ions. It is interesting

(11) (a) Brese, N. E.; O'Keeffe, M. *Acta Crystallogr.* **1991**, *B47*, 192. (b) Brown, I. D.; Altermatt, D. *Acta Crystallogr.* **1985**, *B41*, 244.

Table 2. Important Bond Lengths (Å) for the Six Compounds

$DyCuTe_2O_6Cl$[a]

Dy(1)−O(5)#1	2.302(3)	Dy(1)−O(5)#4	2.370(3)
Dy(1)−O(3)#2	2.307(3)	Dy(1)−O(2)#5	2.407(3)
Dy(1)−O(6)	2.317(3)	Dy(1)−O(1)#5	2.455(3)
Dy(1)−O(2)#3	2.335(3)	Dy(1)−O(4)#4	2.551(3)
Cu(1)−O(1)#6	1.907(3)	Cu(1)−O(6)#6	2.003(3)
Cu(1)−O(4)	1.917(3)	Cu(1)−Cl(1)	2.633(2)
Cu(1)−O(3)	1.991(3)	Te(1)−O(3)	1.879(3)
Te(1)−O(2)	1.879(3)	Te(1)−O(1)	1.894(3)
Te(2)−O(5)	1.870(3)	Te(2)−O(4)	1.896(3)
Te(2)−O(6)	1.875(3)		

$ErCuTe_2O_6Cl$[b]

Er(1)−O(6)#1	2.288(13)	Er(1)−O(3)#5	2.324(14)
Er(1)−O(3)#2	2.303(14)	Er(1)−O(5)	2.383(14)
Er(1)−O(5)#3	2.308(15)	Er(1)−O(4)	2.439(14)
Er(1)−O(2)#4	2.319(13)	Er(1)−O(1)#5	2.557(14)
Cu(1)−O(4)	1.904(14)	Cu(1)−O(2)	1.989(13)
Cu(1)−O(1)#1	1.926(14)	Cu(1)−Cl(1)	2.667(7)
Cu(1)−O(6)#1	1.982(14)	Te(1)−O(3)	1.869(14)
Te(1)−O(2)	1.881(13)	Te(1)−O(1)	1.881(14)
Te(2)−O(6)	1.880(13)	Te(2)−O(5)	1.897(15)
Te(2)−O(4)	1.891(14)		

$ErCuTe_2O_6Br$[b]

Er(1)−O(6)#1	2.292(6)	Er(1)−O(3)#5	2.353(6)
Er(1)−O(3)#2	2.298(6)	Er(1)−O(5)	2.389(6)
Er(1)−O(2)#3	2.301(6)	Er(1)−O(4)	2.455(6)
Er(1)−O(5)#4	2.316(6)	Er(1)−O(1)#5	2.555(7)
Cu(1)−O(4)	1.904(6)	Cu(1)−O(2)	2.011(6)
Cu(1)−O(1)#1	1.907(7)	Cu(1)−Br(1)	2.899(2)
Cu(1)−O(6)#1	1.992(6)	Te(1)−O(3)	1.869(6)
Te(1)−O(2)	1.879(6)	Te(1)−O(1)	1.894(6)
Te(2)−O(5)	1.878(6)	Te(2)−O(4)	1.888(6)
Te(2)−O(6)	1.882(6)		

$Sm_2MnTe_5O_{13}Cl_2$[c]

Sm(1)−O(9)	2.354(4)	Sm(1)−O(4)	2.405(4)
Sm(1)−O(2)#1	2.367(4)	Sm(1)−O(1)#3	2.427(4)
Sm(1)−O(2)	2.370(4)	Sm(1)−O(3)#3	2.553(4)
Sm(1)−O(5)#2	2.387(4)	Sm(1)−O(3)	2.613(4)
Sm(2)−O(10)	2.366(4)	Sm(2)−O(5)	2.431(4)
Sm(2)−O(9)#4	2.404(4)	Sm(2)−O(8)#5	2.445(4)
Sm(2)−O(1)#3	2.405(4)	Sm(2)−O(11)#4	2.479(4)
Sm(2)−O(7)	2.410(4)	Sm(2)−O(4)	2.641(4)
Mn(1)−O(12)#4	2.123(4)	Mn(1)−O(8)#6	2.183(4)
Mn(1)−O(13)	2.126(4)	Mn(1)−O(7)	2.194(4)
Mn(1)−O(10)	2.139(4)	Mn(1)−O(6)#6	2.276(4)
Te(1)−O(1)	1.869(4)	Te(1)−O(3)	1.951(4)
Te(1)−O(2)	1.878(4)	Te(2)−O(5)	1.871(4)
Te(2)−O(4)	1.889(4)	Te(2)−O(3)	2.315(4)
Te(2)−O(6)	2.076(4)	Te(3)−O(8)	1.882(4)
Te(3)−O(7)	1.889(4)	Te(3)−O(6)	1.979(4)
Te(4)−O(10)	1.862(4)	Te(4)−O(11)	1.933(4)
Te(4)−O(9)	1.871(4)	Te(5)−O(12)	1.837(4)
Te(5)−O(13)	1.915(4)	Te(5)−O(11)	2.051(4)
Te(5)−O(13)#7	2.146(4)		

$Dy_2Cu\ Te_5O_{13}Br_2$[d]

Dy(1)−O(2)	2.305(5)	Dy(2)−O(8)	2.302(6)
Dy(1)−O(7)#1	2.311(5)	Dy(2)−O(2)#4	2.365(5)
Dy(1)−O(5)#2	2.323(5)	Dy(2)−O(5)	2.366(5)
Dy(1)−O(7)	2.336(5)	Dy(2)−O(11)#3	2.377(5)
Dy(1)−O(4)	2.377(5)	Dy(2)−O(1)#4	2.405(6)
Dy(1)−O(11)#3	2.379(6)	Dy(2)−O(13)	2.409(6)
Dy(1)−O(9)#3	2.516(5)	Dy(2)−O(3)#5	2.514(5)
Dy(1)−O(9)	2.527(6)	Dy(2)−O(4)	2.555(5)
Cu(1)−O(12)#4	1.995(5)	Cu(1)−O(8)	2.122(6)
Cu(1)−O(3)#6	1.998(5)	Cu(1)−O(13)	2.163(6)
Cu(1)−O(10)	2.072(6)	Cu(1)−O(6)#6	2.320(6)
Te(1)−O(8)	1.854(5)	Te(2)−O(11)	1.884(5)
Te(1)−O(2)	1.875(5)	Te(2)−O(7)	1.891(5)
Te(1)−O(1)	1.936(5)	Te(2)−O(9)	1.945(5)
Te(3)−O(5)	1.877(5)	Te(4)−O(12)	1.836(6)
Te(3)−O(4)	1.889(5)	Te(4)−O(10)	1.931(5)
Te(3)−O(6)	2.058(6)	Te(4)−O(1)	2.067(5)
Te(3)−O(9)	2.356(5)	Te(4)−O(10)#7	2.163(5)
Te(5)−O(13)	1.889(6)	Te(5)−O(6)	1.971(5)
Te(5)−O(3)	1.903(5)		

$Nd_4CuTe_5O_{15}Cl_3$[e]

Nd(1)−O(12)#1	2.391(8)	Nd(1)−O(12)#2	2.391(8)
Nd(1)−O(11)#3	2.489(8)	Nd(1)−O(11)	2.489(8)
Nd(1)−O(10)#3	2.501(8)	Nd(1)−O(10)	2.501(8)
Nd(1)−O(9)#3	2.536(8)	Nd(1)−O(9)	2.536(8)
Nd(2)−O(5)#1	2.399(9)	Nd(2)−O(2)	2.405(8)
Nd(2)−O(9)#3	2.446(8)	Nd(2)−O(7)#2	2.446(8)
Nd(2)−O(12)#2	2.496(9)	Nd(2)−O(11)#1	2.522(8)
Nd(2)−O(10)#2	2.528(9)	Nd(2)−O(6)	2.651(9)
Nd(3)−O(8)#3	2.372(9)	Nd(3)−O(1)#4	2.397(8)
Nd(3)−O(7)#2	2.402(8)	Nd(3)−O(15)#1	2.403(8)
Nd(3)−O(2)	2.423(8)	Nd(3)−O(3)	2.481(9)
Nd(3)−O(14)	2.584(9)	Nd(3)−Cl(3)	2.925(3)
Nd(4)−O(13)#5	2.339(8)	Nd(4)−O(3)	2.344(9)
Nd(4)−O(5)#4	2.395(9)	Nd(4)−O(1)#6	2.459(9)
Nd(4)−O(6)#6	2.488(9)	Nd(4)−O(15)	2.645(8)
Nd(4)−O(4)#4	2.690(9)	Nd(4)−O(14)	2.795(8)
Nd(5)−O(4)	2.410(8)	Nd(5)−O(4)#7	2.410(8)
Nd(5)−O(14)#8	2.435(9)	Nd(5)−O(14)#6	2.435(9)
Nd(5)−O(13)#9	2.465(8)	Nd(5)−O(13)#4	2.465(8)
Nd(5)−O(15)#4	2.585(8)	Nd(5)−O(15)#9	2.585(8)
Cu(1)−Cl(2)	2.296(5)	Cu(1)−Cl(2)#10	2.338(5)
Cu(1)−Cl(1)	2.371(4)	Cu(1)−Cl(3)	2.542(4)
Te(1)−O(1)	1.886(8)	Te(1)−O(2)	1.897(8)
Te(1)−O(3)	1.913(8)	Te(2)−O(6)	1.871(9)
Te(2)−O(4)	1.888(8)	Te(2)−O(5)	1.895(9)
Te(3)−O(7)	1.871(8)	Te(3)−O(8)	1.879(8)
Te(3)−O(9)	1.886(8)	Te(4)−O(12)	1.876(8)
Te(4)−O(10)	1.889(9)	Te(4)−O(11)	1.921(8)
Te(5)−O(13)	1.890(8)	Te(5)−O(14)	1.901(9)
Te(5)−O(15)	1.909(8)		

[a] Symmetry transformations used to generate equivalent atoms. For $DyCuTe_2O_6Cl$: #1 $-x+2, -y, -z$; #2 $x+1, -y+1/2, z-1/2$; #3 $-x+2, y-1/2, -z+1/2$; #4 $x+1, y, z$; #5 $x, -y+1/2, z-1/2$; #6 $x-1, y, z$. [b] For $ErCuTe_2O_6Cl$ and $ErCuTe_2O_6Br$: #1 $x+1, y, z$; #2 $-x, y+1/2, -z-1/2$; #3 $-x, -y+1, -z$; #4 $x, -y+1/2, z+1/2$; #5 $x+1, -y+1/2, z+1/2$. [c] For $Sm_2MnTe_5O_{13}Cl_2$: #1 $-x+2, -y+2, -z$; #2 $x, y+1, z$; #3 $-x+2, -y+1, -z$; #4 $x, y-1, z$; #5 $-x+3/2, y-1/2, -z+1/2$; #6 $-x+3/2, y+1/2, -z+1/2$; #7 $-x+2, -y+2, -z+1$. [d] For $Dy_2Cu\ Te_5O_{13}Br_2$: #1 $-x+1, -y, -z$; #2 $x, y-1, z$; #3 $-x+1, -y+1, -z$; #4 $x, y+1, z$; #5 $-x+1/2, y+1/2, -z+1/2$; #6 $-x+1/2, y-1/2, -z+1/2$; #7 $-x+1, -y, -z+1$. [e] For $Nd_4CuTe_5O_{15}Cl_3$: #1 $x, y+1, z$; #2 $-x, y+1, -z$; #3 $-x, y, -z$; #4 $-x-1/2, y+1/2, -z+1/2$; #5 $-x, y, -z+1$; #6 $-x-1/2, y-1/2, -z+1/2$; #7 $-x-1, y, -z$; #8; $x-1/2, y-1/2, z-1/2$; #9 $x-1/2, y+1/2, z-1/2$; #10 $-x+1/2, y-1/2, -z+1/2$.

to note that the DyO_8 polyhedra are interconnected via edge-sharing (O5−O5) into a 1D dysprosium(III) oxide chain along the *a*-axis (Figure 2a). Each pair of CuO_4Cl polyhedra is bridged by a pair of tellurite groups to form a 1D chain along the *a*-axis (Figure 2b). The interconnection of Dy(III) and Cu(II) ions via bridging tellurite groups lead to a 3D network with apertures running along the *a*-axis (Figure 3). These apertures are formed by 10 polyhedral rings composed of 4 Dy, 4 Cu, and 2 tellurite anions (Figure 3). The chloride anions and the lone pairs of the tellurium(IV) atoms are orientated toward the above apertures. The effective volume of the lone pair is approximately the same as the volume of an O^{2-} anion according to Galy and Andersson.[12]

It should be noted that the structure of $DyCuTe_2O_6Cl$ is

(12) Galy, J.; Meunier, G.; Andersson, S.; Åström, A. *J. Solid State Chem.* **1975**, *13*, 142.

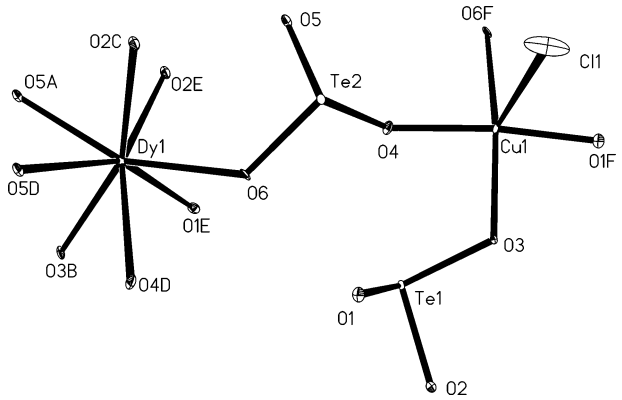

Figure 1. ORTEP representation of the selected unit in $DyCuTe_2O_6Cl$. The thermal ellipsoids are drawn at 50% probability. Symmetry codes for generated atoms: a, $-x + 2, -y, -z$; b, $x + 1, -y + 1/2, z - 1/2$; c, $-x + 2, y - 1/2, -z + 1/2$; d, $x + 1, y, z$; e, $x, -y + 1/2, z - 1/2$; f, $x - 1, y, z$.

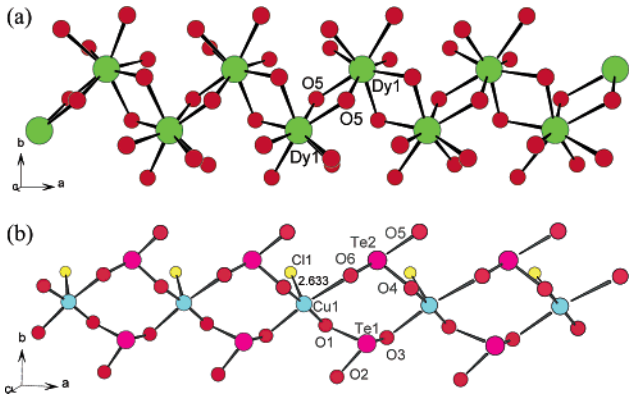

Figure 2. 1D dysprosium(III) oxide chain (a) and a 1D copper(II) tellurite chloride chain (b) along the *a*-axis in $DyCuTe_2O_6Cl$. The CuO_4Cl square pyramids are shaded in cyan. Dy, Cu, Te, Cl, and O atoms are drawn as green, cyan, pink, yellow, and red circles, respectively.

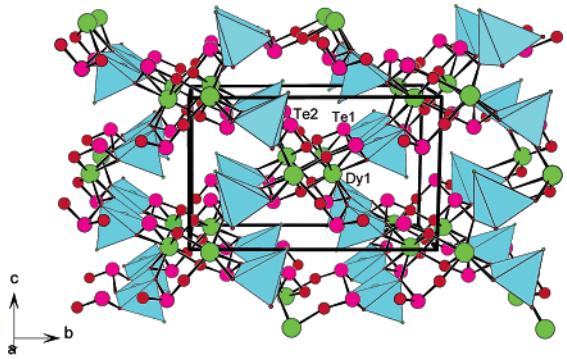

Figure 3. View of the structure of $DyCuTe_2O_6Cl$ down the *a*-axis. The CuO_4Cl square pyramids are shaded in cyan. Dy, Te, and O atoms are drawn as green, pink, and red circles, respectively.

different from those of $SmCo(SeO_3)_2Cl$, $GdCu(SeO_3)_2Cl$, and $SmMn(SeO_3)_2Cl$ although their structural formulas are comparable.[7a] These three lanthanide transition metal selenite chlorides form two different types of 3D network structures in which the chloride anion connects with two transition metal ions and a lanthanide(III) ion. The CoO_4Cl_2 octahedra in $SmCo(SeO_3)_2Cl$ are connected via one edge and one vertex to infinite chains, whereas the linkage of MnO_4Cl_2 octahedra in $SmMn(SeO_3)_2Cl$ to chains occurs exclusively via edge sharing.[7a]

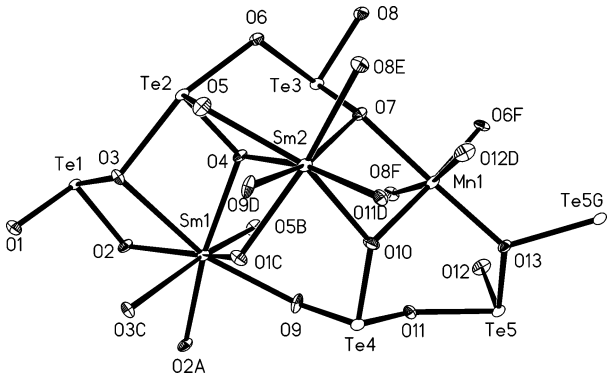

Figure 4. ORTEP representation of the selected unit in $Sm_2Mn(Te_5O_{13})Cl_2$. The thermal ellipsoids are drawn at 50% probability. The noncoordination chloride anions are omitted for clarity. Symmetry codes for generated atoms: a, $-x + 2, -y + 2, -z$; b, $x, y + 1, z$; c, $-x + 2, -y + 1, -z$; d, $x, y - 1, z$; e, $-x + 3/2, y - 1/2, -z + 1/2$; f, $-x + 3/2, y + 1/2, -z + 1/2$; g, $-x + 2, -y + 2, -z + 1$.

$Sm_2MnTe_5O_{13}Cl_2$ and $Dy_2CuTe_5O_{13}Br_2$ are isostructural, and their structures feature a 3D network with long, narrow-shaped tunnels occupied by the isolated halides. The structure of $Sm_2MnTe_5O_{13}Cl_2$ will be discussed in detail as representative of all structures. The synthesis of $Sm_2MnTe_5O_{13}Cl_2$ can be expressed by the following reaction at 700 °C: $Sm_2O_3 + MnCl_2 + 5TeO_2 \rightarrow Sm_2MnTe_5O_{13}Cl_2$. As shown in Figure 4, both Sm(III) ions in the asymmetric unit are eight-coordinated by eight oxygens with Sm−O distances ranging from 2.354(4) to 2.641(4) Å, comparable to those reported in other related compounds.[7a] The Mn(II) ion is octahedrally coordinated by six oxygen atoms. The Mn−O distances vary from 2.123(4) to 2.276(4) Å. In addition to ψ-TeO_3 tetrahedral coordination geometry as in $DyCuTe_2O_6Cl$, ψ-TeO_4 square pyramids with the lone-pair electrons occupying the pyramidal position are also found in $Sm_2MnTe_5O_{13}Cl_2$. These two types of polyhedra are further interconnected via corner and edge sharing to form two different tellurium(IV) oxide anions: $Te_3O_8^{4-}$ and $Te_4O_{10}^{4-}$ (Figure 4). Hence, $Sm_2MnTe_5O_{13}Cl_2$ can be also formulated as $Sm_4Mn_2(Te_3O_8)_2(Te_4O_{10})Cl_4$. In addition to $Te_3O_8^{4-}$ and $Te_4O_{10}^{4-}$ anions found in $Sm_2MnTe_5O_{13}Cl_2$, the Te(IV) ion also forms several other units such as the $Te_2O_6^{4-}$ anion in $CeTe_2O_6$ and the linear $Te_4O_{11}^{6-}$ anion in $Ln_2Te_4O_{11}$ (Ln = La−Lu).[1,6] In $Te_4O_{10}^{4-}$, two TeO_4 form a dimeric unit by edge sharing, and the dimer further corner shares with two TeO_3 groups. $Te_3O_8^{4-}$ is composed of three corner-sharing TeO_3 groups. The Te−O distances of the Te−O−Te bridge (1.915(4)−2.315(4) Å) are significantly longer than the remaining Te−O bonds (1.837(4)−1.889(4) Å) (Table 2). The bond valence calculations indicate that all of the Te atoms are 4+; the calculated total bond valences for Te(1), Te(2), Te(3), Te(4), and Te(5) are 3.72, 3.77, 3.56, 3.82, and 4.09, respectively.[11]

The $Te_4O_{10}^{4-}$ anion chelates bidentately with two Sm(2) atoms (two O−Te−O−Sm four-membered rings) and two Mn(1) (two O−Te−O−Te−O−Mn six-membered rings) and also bridges to two Sm(1), two Sm(2), and two Mn(1) atoms (Figure 5a). The $Te_3O_8^{4-}$ anion chelates tridentately with one Sm(1) (O2, O3, O4) and one Sm(2) (O4, O5, O7), bidentately

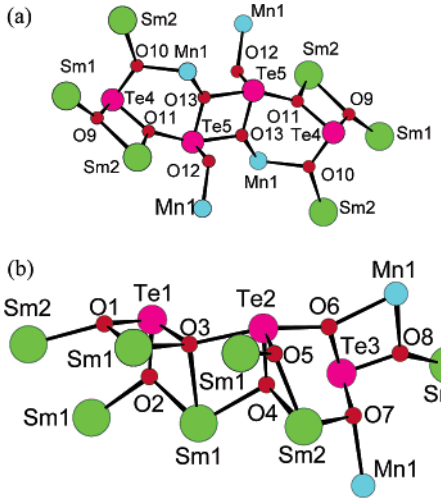

Figure 5. Coordination modes of $Te_4O_{10}^{4-}$ (a) and $Te_3O_8^{4-}$ anion in $Sm_2Mn(Te_5O_{13})Cl_2$. Sm, Mn, Te, and O atoms are drawn as green, cyan, pink, and red circles, respectively.

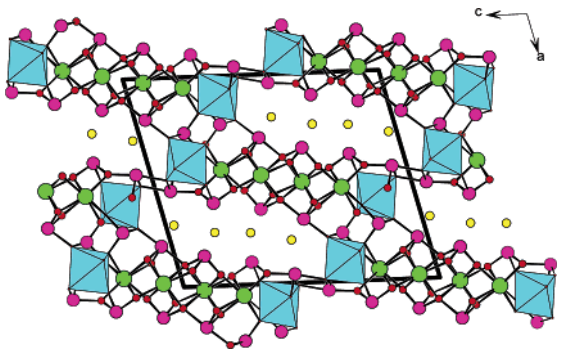

Figure 6. View of the structure of $Sm_2Mn(Te_5O_{13})Cl_2$ down the *b*-axis. The MnO_6 tetrahedra are shaded in cyan. Sm, Te, Cl, and O atoms are drawn as green, pink, yellow, and red circles, respectively.

with one Sm(1) (O1, O3) and one Mn(1) (O6, O8), and also bridges with one Sm(1), two Sm(2), and one Mn(1) (Figure 5b). The interconnection of the Sm^{III} ions and Mn^{II} ions by $Te_3O_8^{4-}$ and $Te_4O_{10}^{4-}$ anions results in a 3D network with tunnels running along the *b*-axis (Figure 6). The chloride anions remain isolated and are located at the above tunnels. The lone-pair electrons of the tellurium(IV) atoms are also oriented toward the tunnels (Figure 6). It is noticed that the structure of $Sm_2MnTe_5O_{13}Cl_2$ contains 1D slabs of samarium oxide along the *b*-axis in which the SmO_8 polyhedra are interconnected through edge sharing (Figure 7a), and $\langle\bar{2}02\rangle$ layers of Mn−Te−O in which the Mn(II) ions are bridged by a pair of TeO_4 or TeO_3 groups, resulting in Mn_2Te_2 and Mn_3Te_3 polyhedral rings (Figure 7b).

$Nd_4Cu(TeO_3)_5Cl_3$ was initially obtained in our attempts to prepare the Nd(III) analogue of $DyCuTe_2O_6Cl$. It was found that the Cu(II) ion has been reduced to the Cu(I) ion by reducing TeO_2 (which is oxidized to be tellurate anion). After structural analysis, $Nd_4Cu(TeO_3)_5Cl_3$ was then obtained as a single phase by applying the Cu(I) source directly at 650 °C: $2NdOCl + Nd_2O_3 + CuCl + 5TeO_2 \rightarrow Nd_4CuTe_5O_{15}Cl_3$.

The structure of $Nd_4Cu(TeO_3)_5Cl_3$ features a 3D network of neodymium(III) tellurite with large tunnels in which 1D chains of copper(I) chloride are inserted (Figure 8a). Among

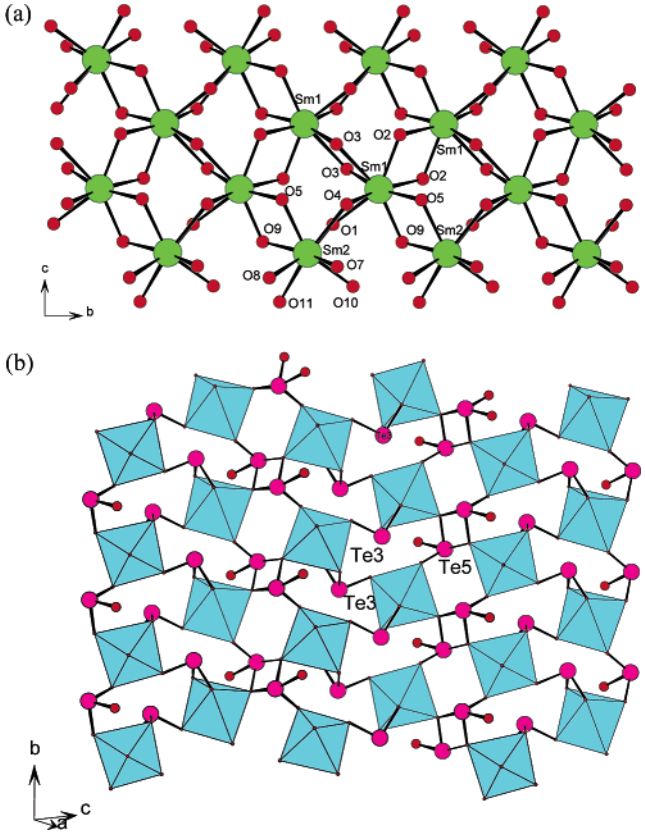

Figure 7. 1D samarium(III) oxide slab (a) and a $\langle\bar{2}02\rangle$ manganese(II) tellurium(IV) oxychloride layer in $Sm_2Mn(Te_5O_{13})Cl_2$. The MnO_6 octahedra are shaded in cyan. Sm, Te, and O atoms are drawn as green, pink, and red circles, respectively.

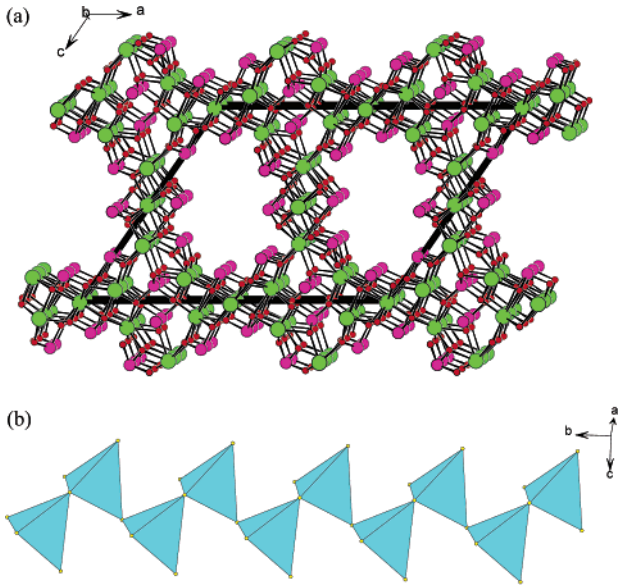

Figure 8. A 3D network of neodymium(III) tellurite with tunnels along the *b*-axis (a) and a 1D zigzag copper(I) chloride tetrahedral chain along the *b*-axis in $Nd_4Cu(TeO_3)_5Cl_3$. Nd, Te, and O atoms are drawn as green, pink, and red circles, respectively. The $CuCl_4$ tetrahedra are shaded in cyan.

the five Nd(III) ions in an asymmetric unit, four of them (Nd(1), Nd(2), Nd(4), and Nd(5)) are eight-coordinated by eight oxygen atoms. Nd(3) is eight-coordinated by seven tellurite oxygens and a chloride anion. The Nd−O distances are in the range of 2.339(8)−2.795(8) Å, which are com-

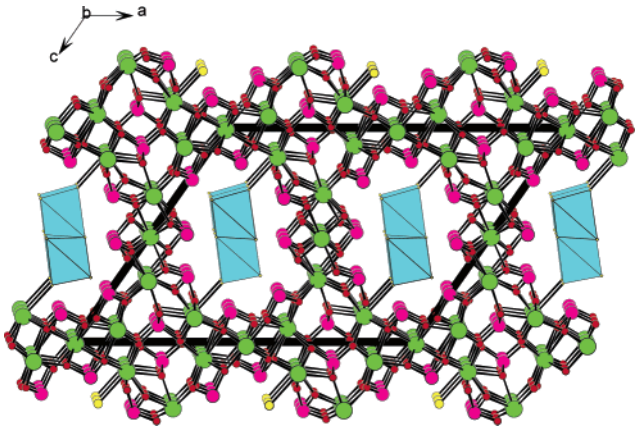

Figure 9. View of the structure of $Nd_4Cu(TeO_3)_5Cl_3$ down the *b*-axis. The $CuCl_4$ tetrahedra are shaded in cyan. Nd, Te, Cl, and O atoms are drawn as green, pink, yellow, and red circles, respectively.

parable to those reported in other neodymium(III) tellurium(IV) oxides.[13] The Nd−Cl distance of 2.925(3) Å is significantly longer than that of the Nd−O bonds. The Cu(I) ion is tetrahedrally coordinated by four chloride anions. The Cu−Cl distances ranges from 2.296(5) to 2.542(4) Å (Table 2). All five of the Te atoms adopt the same coordination geometry as those in $DyCuTe_2O_6Cl$, $ErCuTe_2O_6Cl$, and $ErCuTe_2O_6Br$. The Te−O distances are in the range of 1.871(8)−1.921(8) Å, which are comparable to those in $DyCuTe_2O_6Cl$, $ErCuTe_2O_6Cl$, and $ErCuTe_2O_6Br$. The oxidation states of Cu and Te are 1+ and 4+, respectively, which are also supported by the results of bond valence calculations.[11] The calculated total bond valences for Cu(1), Te(1), Te(2), Te(3), Te(4), and Te(5) are 0.97, 3.85, 3.69, 3.91, 3.71, and 3.75, respectively.

The five tellurite groups adopt four different coordination modes. $Te(1)O_3$ and $Te(2)O_3$ groups each chelate a Nd(III) ion bidentately and also bridge to four other Nd(III) ions. The $Te(3)O_3$ group bridges to five Nd(III) ions. The $Te(4)O_3$ group chelates with two Nd(III) ions bidentately and also bonds with two other Nd(III) ions. $Te(5)O_3$ group chelates with two Nd(III) ions bidentately and also bonds to four other Nd(III) ions. The interconnection of Nd(III) ions by bridging and chelating tellurite groups leads to a 3D network with large tunnels along the *b*-axis (Figure 8a). The tunnels are formed by 16-membered polyhedral rings composed of 8 TeO_3 and 8 Nd atoms. The lone-pair electrons of the tellurite groups are located at the above tunnels. Neighboring $CuCl_4$ tetrahedra are interconnected via corner sharing into a 1D two-unit repeating (zweier) chain along the *b*-axis (Figure 8b). These copper(I) chloride chains are inserted in the centers of the above tunnels, forming Cu−Cl−Nd bridges (Figure 9).

Luminescent Properties. The near-IR solid-state luminescent properties of $ErCu(TeO_3)_2Cl$ and $Nd_4Cu(TeO_3)_5Cl_3$ were investigated at room temperature. Under excitation at 584 nm, $Nd_4Cu(TeO_3)_5Cl_3$ displays the characteristic emission bands for the Nd(III) ion: an emission band at 879 nm ($^4F_{3/2} \rightarrow {}^4I_{9/2}$), a strong emission band at 1067 nm ($^4F_{3/2} \rightarrow {}^4I_{11/2}$), and a weak band at 1343 nm ($^4F_{3/2} \rightarrow {}^4I_{13/2}$) in the near-IR region (Figure 10).[13] The emission spectrum of $ErCu(TeO_3)_2Cl$ under excitation at 808 nm shows two very strong bands at 1540 and 1561 nm as well as two shoulder bands at 1498 and 1603 nm. All of these four bands can be attributed to the $^4I_{13/2} \rightarrow {}^4I_{15/2}$ transition band,[14] which is split into several close bands by the low symmetry (*C*1) around the erbium(III) ion.

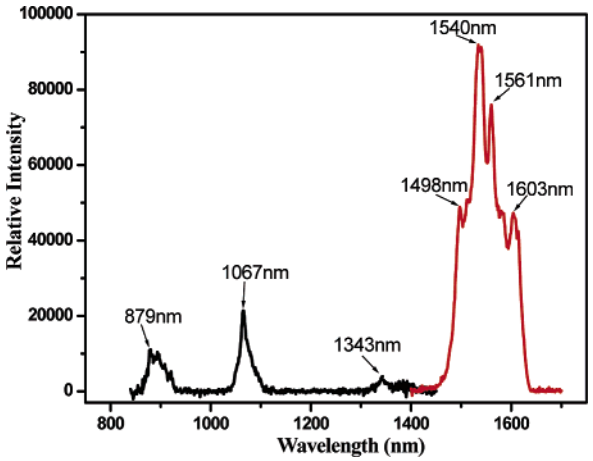

Figure 10. Emission spectrum of $ErCuTe_2O_6Cl$ under excitation at λ_{ex} = 808 nm (red) and that of $Nd_4Cu(TeO_3)_5Cl_3$ under excitation at λ_{ex} = 584 nm (black).

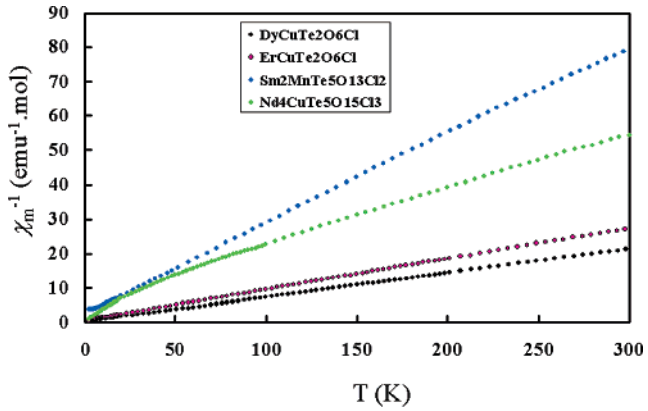

Figure 11. Plots of χ_m^{-1} vs temperature (*T*) for $DyCuTe_2O_6Cl$, $ErCuTe_2O_6Cl$, $Sm_2Mn(Te_5O_{13})Cl_2$, and $Nd_4Cu(TeO_3)_5Cl_3$.

Magnetic Properties. Magnetic properties for $DyCuTe_2O_6Cl$, $ErCuTe_2O_6Cl$, $Sm_2Mn(Te_5O_{13})Cl_2$, and $Nd_4Cu(TeO_3)_5Cl_3$ have been studied at a magnetic field of 10 000 Oe in the temperature range of 2−300 K. The plots of χ_m^{-1} vs temperature (*T*) are shown in Figure 11; $DyCuTe_2O_6Cl$ and $ErCuTe_2O_6Cl$ obey Curie−Weiss law in the whole experimental temperature region, whereas $Sm_2Mn(Te_5O_{13})Cl_2$ obeys between 20 and 300 K and $Nd_4Cu(TeO_3)_5Cl_3$ above

(13) (a) Castro, A.; Enjalbert, R.; Lloyd, D.; Rasines, I.; Galy, J. *J. Solid State Chem.* **1990**, *85*, 100. (b) Tarasov, I. V.; Dolgikh, V. A.; Aksel'rud, L. G.; Berdonosov, P. S.; Ponovkin, B. A. *Zh. Neorg. Khim.* **1996**, *41*, 1243. (c) Nikiforov, G. B.; Kusainova, A. M.; Berdonosov, P. S.; Dolgikh, V. A.; Lightfoot, P. *J. Solid State Chem.* **1999**, *146*, 473. (d) Berdonosov, P. S.; Charkin, D. O.; Kusainova, A. M.; Hervoches, C. H.; Dolgikh, V. A.; Lightfoot, P. *Solid State Sci.* **2000**, *2*, 553.

(14) (a) Song, J.-L.; Lei, C.; Mao, J.-G. *Inorg. Chem.* **2004**, *43*, 5630. (b) Hebbink, G. A.; Grave, L.; Woldering, L. A.; Reinhoudt, D. N.; van Vegel, F. C. J. M. *J. Phys. Chem.* **2003**, *A107*, 2483. (c) Faulkner, S.; Pope, S. J. A. *J. Am. Chem. Soc.* **2003**, *125*, 10526. (d) Pope, S. J. A.; Kenwright, A. M.; Boote, V. A.; Faulkner, S. *J. Chem. Soc., Dalton Trans.* **2003**, 3780.

100 K. At 300 K, the effective magnetic moments (μ_{eff}) are calculated to be 10.65, 9.44, 5.51, and 6.74 μ_B, respectively, for $DyCuTe_2O_6Cl$, $ErCuTe_2O_6Cl$, $Sm_2Mn(Te_5O_{13})Cl_2$, and $Nd_4Cu(TeO_3)_5Cl_3$, which are slightly smaller than the theoretical values (10.74, 9.75, 6.33, and 7.36 μ_B, respectively). At 2 K, the $\chi_m T$ values are decreased to 2.92, 3.48, 0.52, and 2.08 emu·K·mol^{-1}, respectively, for $DyCuTe_2O_6Cl$, $ErCuTe_2O_6Cl$, $Sm_2Mn(Te_5O_{13})Cl_2$, and $Nd_4Cu(TeO_3)_5Cl_3$, indicating the antiferromagnetic interactions between magnetic centers.

Linear fitting of χ_m^{-1} with T above 100 K gave Weiss constants of −3.2(2), −10.1(2), −18.8(3), and −48.2(4) K, respectively, for $DyCuTe_2O_6Cl$, $ErCuTe_2O_6Cl$, $Sm_2Mn(Te_5O_{13})Cl_2$, and $Nd_4Cu(TeO_3)_5Cl_3$. For $DyCuTe_2O_6Cl$, $ErCuTe_2O_6Cl$, and $Sm_2Mn(Te_5O_{13})Cl_2$, the magnetic interactions are mainly between lanthanide(III) ions as well as between the lanthanide(III) ion and transition metal ion (TM). The shortest Ln−Ln and Ln−TM distances are 3.763(1) and 3.370 (1) Å for $DyCuTe_2O_6Cl$, 3.755(1) and 3.362 (1) Å for $ErCuTe_2O_6Cl$, and 3.891(1) and 3.417(1) Å for $Sm_2Mn(Te_5O_{13})Cl_2$, respectively. The distances between transition metal centers are much longer (5.392(1), 5.385(1), and 5.741(1) Å, respectively, for $DyCuTe_2O_6Cl$, $ErCuTe_2O_6Cl$, and $Sm_2Mn(Te_5O_{13})Cl_2$); hence, Cu···Cu magnetic interactions for $DyCuTe_2O_6Cl$ and $ErCuTe_2O_6Cl$ are expected to be weak, but Mn···Mn magnetic interactions for $Sm_2Mn(Te_5O_{13})Cl_2$ still can make significant contribution, which is supported by its much more negative Weiss constant. For $Nd_4Cu(TeO_3)_5Cl_3$, since the copper(I) ion is diamagnetic, only Nd−Nd magnetic interactions are possible, and the shortest Nd−Nd distance is 3.904(1) Å. More detailed calculations of these magnetic interactions were not performed because of the complexity of the structures as well as the lack of suitable models.

Conclusion

In summary, the syntheses, crystal structures, and magnetic and luminescent properties of six new rare-earth transition metal tellurium(IV) oxyhalides have been described. The halide anion can be unidentate (in $DyCuTe_2O_6Cl$, $ErCuTe_2O_6Cl$, and $ErCuTe_2O_6Br$), be bidentate as in $Nd_4Cu(TeO_3)_5Cl_3$, or remain isolated in $Sm_2MnTe_5O_{13}Cl_2$ and $Dy_2CuTe_5O_{13}Br_2$. It is interesting to note that the copper(I) chloride tetrahedra in $Nd_4Cu(TeO_3)_5Cl_3$ form a 1D two-unit repeating (zweier) chain via corner sharing, and such chains are inserted in the tunnels of lanthanide(III) tellurite. Furthermore, two types of polymeric tellurium(IV) oxide anions are formed in $Sm_2MnTe_5O_{13}Cl_2$ and $Dy_2CuTe_5O_{13}Br_2$: $Te_3O_8^{4-}$ and $Te_4O_{10}^{4-}$. $ErCu(TeO_3)_2Cl$ and $Nd_4Cu(TeO_3)_5Cl_3$ exhibit strong emission bands in the near-IR region. Magnetic property measurements for $DyCuTe_2O_6Cl$, $ErCuTe_2O_6Cl$, $Sm_2Mn(Te_5O_{13})Cl_2$, and $Nd_4Cu(TeO_3)_5Cl_3$ show the antiferromagnetic interactions between magnetic centers. It is anticipated that many other new lanthanide transition metal tellurium(IV) oxyhalides with interesting structures as well as physical properties will be discovered in similar systems.

Acknowledgment. This work was supported by the National Natural Science Foundation of China (No. 20371047) and NSF of Fujian Province (No. E0420003).

Supporting Information Available: X-ray crystallographic files for $DyCuTe_2O_6Cl$, $ErCuTe_2O_6Cl$, $ErCuTe_2O_6Br$, $Sm_2Mn(Te_5O_{13})Cl_2$, $Dy_2CuTe_5O_{13}Br_2$, and $Nd_4Cu(TeO_3)_5Cl_3$ in CIF format and XRD powder patterns for $DyCuTe_2O_6Cl$, $ErCuTe_2O_6Cl$, $Sm_2Mn(Te_5O_{13})Cl_2$, and $Nd_4Cu(TeO_3)_5Cl_3$. This material is available free of charge via the Internet at http://pubs.acs.org.

IC050420V